variation and possibly the between-genome G+C% differences of eukaryotes. In addition, the nucleosome-derived within-genome G+C% variations in turn can be used to predict the nucleosome profiles (*20*).

Spontaneous mutations are not randomly distributed in a eukaryotic genome, although the underlying mechanism is poorly understood (*1*, *21*, *22*). We have revealed that nucleosomes, the most abundant eukaryotic protein-DNA complexes (*7*), likely function as a major regulator of substitution mutations in eukaryotes. Binding of proteins to DNA to suppress DNA breathing or to exclude endogenous mutagens may be how cells protect their DNA (*23*). However, DNA repair, which often works with varied efficiency between nucleosomal DNA and naked DNA (*24*), may also shape the base-specific mutation spectrum. Confounding factors such as recombination rate (*25*) and replication timing (*26*) that covary with chromatin status and affect all types of mutations cannot explain our observation, because not all mutation types show an NOS-dependent trend (Fig. 3). Regardless of the underlying mechanisms, the observed nucleosome-dependent mutation spectra have implications for understanding eukaryotic genome structure and evolution, such as the isochore structure (*27*), as well as somatic mutations in cancers and in induced pluripotent stem cells, both of which are associated with chromatin remodeling (*28*, *29*). They also suggest that conventional mutation models widely used in evolutionary analyses are oversimplified (fig. S7).

References and Notes

1. C. F. Baer, M. M. Miyamoto, D. R. Denver, *Nat. Rev. Genet.* **8**, 619 (2007).
2. H. Maki, *Annu. Rev. Genet.* **36**, 279 (2002).
3. J. W. Drake, *Annu. Rev. Genet.* **25**, 125 (1991).
4. M. Lynch *et al.*, *Proc. Natl. Acad. Sci. U.S.A.* **105**, 9272 (2008).
5. K. J. Fryxell, E. Zuckerkandl, *Mol. Biol. Evol.* **17**, 1371 (2000).
6. M. Guéron, M. Kochoyan, J. L. Leroy, *Nature* **328**, 89 (1987).
7. C. Jiang, B. F. Pugh, *Nat. Rev. Genet.* **10**, 161 (2009).
8. D. S. Gross, W. T. Garrard, *Annu. Rev. Biochem.* **57**, 159 (1988).
9. Materials and methods are available as supporting material on *Science* Online.
10. K. J. Impellizzeri, B. Anderson, P. M. Burgers, *J. Bacteriol.* **173**, 6807 (1991).
11. J. H. Proffitt, J. R. Davie, D. Swinton, S. Hattman, *Mol. Cell. Biol.* **4**, 985 (1984).
12. S. Sasaki *et al.*, *Science* **323**, 401 (2009).
13. S. Ercan, Y. Lubling, E. Segal, J. D. Lieb, *Genome Res.* **21**, 237 (2011).
14. M. Lynch, J. S. Conery, *Science* **302**, 1401 (2003).
15. A. Martinez, R. Kolter, *J. Bacteriol.* **179**, 5188 (1997).
16. K. P. Weber *et al.*, *PLoS ONE* **5**, e13922 (2010).
17. V. Iyer, K. Struhl, *EMBO J.* **14**, 2570 (1995).
18. E. Segal, J. Widom, *Curr. Opin. Struct. Biol.* **19**, 65 (2009).
19. N. Kaplan *et al.*, *Nature* **458**, 362 (2009).
20. D. Tillo, T. R. Hughes, *BMC Bioinformatics* **10**, 442 (2009).
21. N. Arnheim, P. Calabrese, *Nat. Rev. Genet.* **10**, 478 (2009).
22. K. H. Wolfe, P. M. Sharp, W. H. Li, *Nature* **337**, 283 (1989).
23. A. Sohail, C. S. Hayes, P. Divvela, P. Setlow, A. S. Bhagwat, *Biochemistry* **41**, 11325 (2002).
24. Y. Ataian, J. E. Krebs, *Biochem. Cell Biol.* **84**, 490 (2006).
25. I. V. Getun, Z. K. Wu, A. M. Khalil, P. R. Bois, *EMBO Rep.* **11**, 555 (2010).
26. C. L. Chen *et al.*, *Genome Res.* **20**, 447 (2010).
27. G. Bernardi, *Annu. Rev. Genet.* **23**, 637 (1989).
28. G. L. Dalgliesh *et al.*, *Nature* **463**, 360 (2010).
29. K. Takahashi *et al.*, *Cell* **131**, 861 (2007).

Acknowledgments: We thank J. Zhang, M. Bakewell, W. Qian, and C.-I. Wu for comments and critical reading of the manuscript. This work was supported by research grants from the National Basic Research Program of China (no. 2010CB126200), the National Natural Science Foundation of China (no. 40930212), and the Science and Technology Planning Project of Guangdong Province (no. 2009B080701090). Data are deposited in NCBI Short Read Archive (SRA040058).

Supporting Online Material

www.sciencemag.org/cgi/content/full/335/6073/1235/DC1
Materials and Methods
Figs. S1 to S10
Tables S1 to S3
References (*30*–*36*)

6 December 2011; accepted 30 January 2012
10.1126/science.1217580

Unique Processing During a Period of High Excitation/Inhibition Balance in Adult-Born Neurons

Antonia Marín-Burgin,* Lucas A. Mongiat,* M. Belén Pardi,* Alejandro F. Schinder†

The adult dentate gyrus generates new granule cells (GCs) that develop over several weeks and integrate into the preexisting network. Although adult hippocampal neurogenesis has been implicated in learning and memory, the specific role of new GCs remains unclear. We examined whether immature adult-born neurons contribute to information encoding. By combining calcium imaging and electrophysiology in acute slices, we found that weak afferent activity recruits few mature GCs while activating a substantial proportion of the immature neurons. These different activation thresholds are dictated by an enhanced excitation/inhibition balance transiently expressed in immature GCs. Immature GCs exhibit low input specificity that switches with time toward a highly specific responsiveness. Therefore, activity patterns entering the dentate gyrus can undergo differential decoding by a heterogeneous population of GCs originated at different times.

The adult hippocampus continuously generates new neurons that integrate in the dentate gyrus network and become relevant for information processing during specific learning tasks (*1*–*7*). Experimental manipulations that reduce adult neurogenesis produce impairment of hippocampus-dependent learning and behavior (*8*, *9*). Yet, the specific traits that determine the functional relevance of adult-born neurons remain unknown (*10*, *11*). Is it solely the continuous addition of new neurons to the network that is important, or are there specific functional properties only attributable to new granule cells (GCs) that are relevant to information processing?

When reaching maturity, adult-born GCs exhibit functional properties that are indistinguishable from GCs generated during development (*3*). However, while developing, immature GCs display elevated intrinsic excitability, reduced γ-aminobutyric acid (GABA)–mediated inhibition, and enhanced capacity to undergo activity-dependent synaptic potentiation (*12*–*16*). Such high intrinsic excitability would potentially allow immature GCs to be activated by entorhinal afferents in spite of their low density of glutamatergic inputs (*17*). It has thus recently been hypothesized that immature GCs might be critical to hippocampal function (*18*–*20*).

First, we investigated how immature GCs process afferent activity from entorhinal inputs and how they compare with mature GCs in the adult mouse hippocampus. We selected 4-week-old neurons because this is the earliest stage at which adult-born GCs can be reliably activated by an excitatory drive (*17*). Adult-born GCs were retrovirally labeled to express red fluorescent protein (RFP), and acute hippocampal slices were prepared 4 weeks post retroviral injection (4 WPI). Time-lapse calcium imaging was performed by using Oregon Green 1,2-bis(2-aminophenoxy)ethane-*N*,*N*,*N*′,*N*′-tetraacetic acid (BAPTA)–1 AM (OGB-1AM) to monitor the activation of immature (4 WPI, RFP^+) and mature (RFP^-) GCs in response to medial perforant path (mPP) stimulation [Fig. 1, A to D; fig. S1; and supporting online material (SOM)]. Ensemble maps representing active neuronal populations were obtained at increasing input strengths (Fig. 1E and fig. S2, A to C). The number of active immature and mature GCs increased with stronger stimuli. Each stimulus

Laboratorio de Plasticidad Neuronal, Instituto Leloir, Instituto de Investigaciones Bioquímicas de Buenos Aires–Consejo Nacional de Investigaciones Científicas y Técnicas (CONICET), Avenida Patricias Argentinas 435, 1405 Buenos Aires, Argentina.

*These authors contributed equally to this work.
†To whom correspondence should be addressed. E-mail: aschinder@leloir.org.ar

consistently activated a larger proportion of the immature GC population (Fig. 1F), suggesting that immature neurons require weaker inputs to trigger a spike.

We used electrophysiological recordings to dissect the mechanisms involved in the differential activation of immature and mature GCs. We characterized the activation profile of GCs at the single-cell level using loose patch recordings in order to detect spikes in response to mPP activation (Fig. 2, A to C). Stimuli of increasing intensity elicited spikes with increasing probability in all GCs, yet mature GCs demanded stronger inputs in order to spike. We measured the input strength required to elicit 50% spiking probability (hereafter called threshold input) (Fig. 2C and SOM). A cumulative distribution of the threshold inputs was then used to build the activation curves, which represent the fractional recruitment of the GC populations as a function of the input strength (Fig. 2D). The activation curve corresponding to mature GCs is shifted toward higher input strengths with respect to immature neurons. As an example, a stimulus that recruits ~5% of mature neurons activates ~30% of immature GCs.

These data indicate that the dentate gyrus comprises a heterogeneous population of GCs in which different subpopulations display diverse activation thresholds and support the observations obtained by using immediate early gene expression that adult-born neurons could participate in information processing in hippocampus-dependent tasks (*5*, *21*, *22*). To investigate how immature and mature GCs respond to conditions of activity that resemble those occurring during hippocampus-dependent behaviors (*23*), we measured spiking in response to 10-Hz trains delivered to the mPP. We found that immature GCs fire repeatedly during the train, whereas mature GCs fire at most a single spike (Fig. 2, F and G). Our results suggest that immature GCs might be activated during behavior by entorhinal inputs with higher probability than that of mature GCs.

The high intrinsic excitability of immature GCs is sufficient to compensate for their weak glutamatergic inputs but does not predict their lower threshold input for activation (*17*). However, mPP axons not only produce monosynaptic glutamatergic excitation of GCs, they also recruit in a feed-forward manner GABAergic inhibitory circuits, which can modulate neuronal firing in response to afferent inputs (*24*–*26*). We therefore investigated the role of inhibition in the activation of GCs. Blocking GABAergic inhibition with picrotoxin (PTX) induced a significant reduction in the input strength required to activate mature but not immature GCs (Fig. 2, C to E).

The developmental GABA switch from depolarizing to hyperpolarizing occurs in adult-born neurons (*27*). The inhibitory nature of GABAergic inputs in 4-WPI GCs was corroborated by means of perforated patch recordings and rendered hyperpolarized values of GABA reversal potential for all GCs (fig. S3). We then investigated the precise contribution of excitatory and inhibitory components that control the activation of GCs. We activated mPP axons and measured the threshold input of GCs in loose patch recordings. Subsequently, we performed whole-cell recordings in the same neurons to measure excitatory and inhibitory responses elicited at threshold input (Fig. 3A and fig. S4). Activation of mPP produced excitatory postsynaptic currents (EPSCs) and inhibitory postsynaptic currents (IPSCs), indicating that glutamatergic entorhinal axons directly activate immature and mature GCs and also recruit inhibitory interneurons that synapse into both populations. Yet, the maximal conductance of both excitatory and inhibitory responses (EPSG and IPSG) was

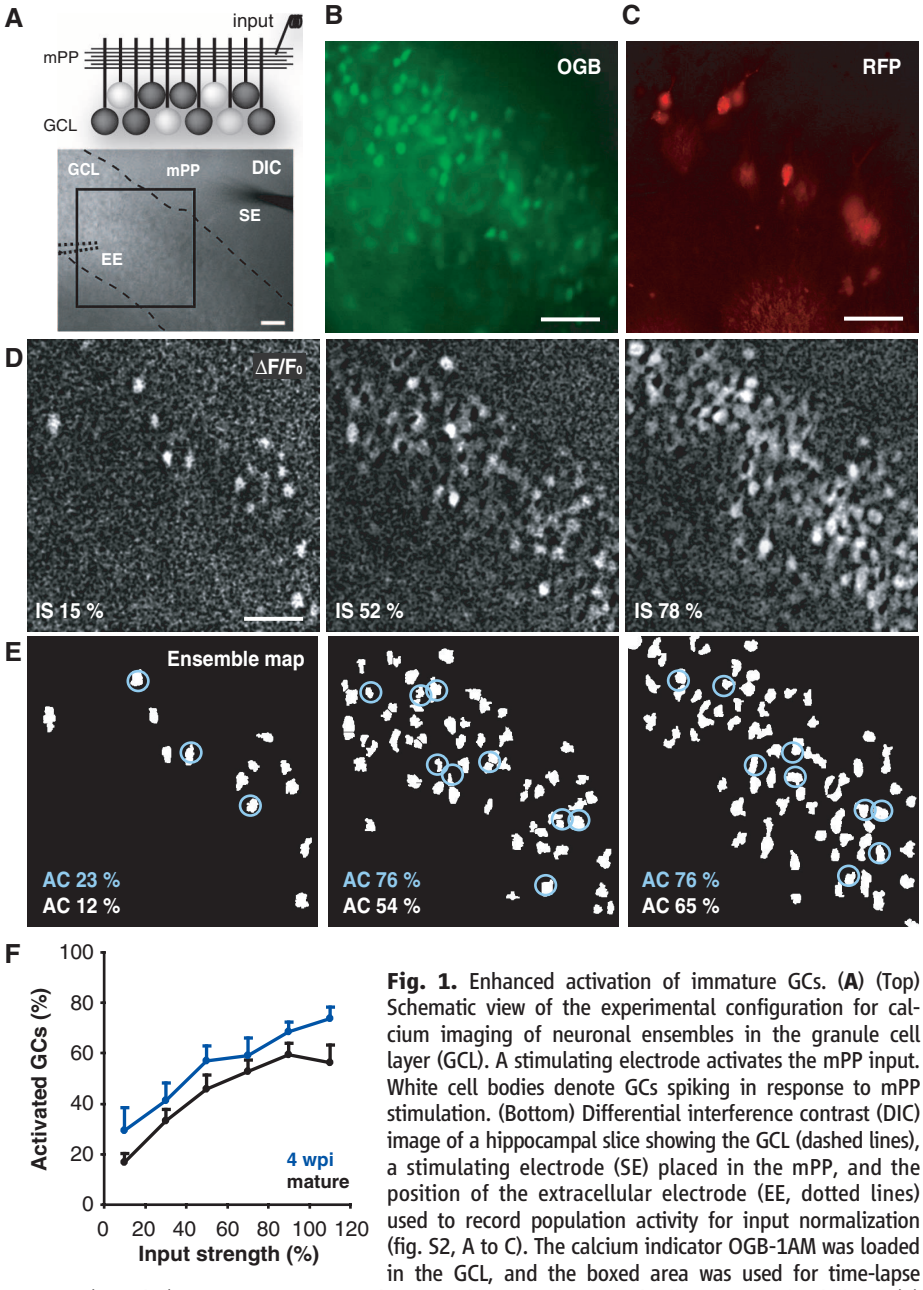

Fig. 1. Enhanced activation of immature GCs. (**A**) (Top) Schematic view of the experimental configuration for calcium imaging of neuronal ensembles in the granule cell layer (GCL). A stimulating electrode activates the mPP input. White cell bodies denote GCs spiking in response to mPP stimulation. (Bottom) Differential interference contrast (DIC) image of a hippocampal slice showing the GCL (dashed lines), a stimulating electrode (SE) placed in the mPP, and the position of the extracellular electrode (EE, dotted lines) used to record population activity for input normalization (fig. S2, A to C). The calcium indicator OGB-1AM was loaded in the GCL, and the boxed area was used for time-lapse imaging. (**B** and **C**) Larger magnification depicting the imaged area with all OGB-1AM–loaded GCs (B) and 4-WPI (RFP^+) GCs (C). (**D**) Representative experiment displaying neuronal ensembles activated at increasing input strengths [IS, assessed as percent field excitatory postsynaptic potential slope ($fEPSP_{slope}$)] (fig. S2, A to C, and SOM). Images are averages of peak $\Delta F/F_0$ of 5 trials from the same slice shown in (A) to (C). (**E**) Ensemble maps corresponding to the panels shown in (D) (fig. S1 and SOM). The percentage of active cells (ACs) is indicated for mature (RFP^-, white labels) or 4-WPI GCs (RFP^+, circled cells, blue labels). (**F**) Percentage of activated cells as a function of input strength. Immature GCs (n = 4 to 14 slices per bin) displayed higher levels of activation than those of mature GCs (n = 5 to 18 slices per bin) [$P < 0.01$, two-way analysis of variance (ANOVA)]. Data was binned every 20% input strength. Scale bars, 50 μm.

substantially larger in mature GCs (Fig. 3, A to C), maintaining a similar ratio of peak excitation/inhibition and reflecting the higher density of glutamatergic and GABAergic contacts characteristic of fully developed neurons (*3*, *14*). Four-WPI neurons displayed a significant delay in the onset of inhibition, which occurred at a time that followed spiking in those cells (Fig. 3, B and D). Thus, it is very unlikely that spike initiation in immature GCs is controlled by inhibitory circuits. We then hypothesized that the observed difference in the activation threshold relied on the excitation/inhibition balance at the precise moment of spiking. Indeed, excitation onto immature GCs (~4 nS) was about fourfold that of inhibition at the moment of spiking (~1 nS), whereas that ratio was twofold in mature GCs (~6 and ~3 nS) (Fig. 3E). To determine whether this difference was due to the slow maturation of perisomatic GABAergic synapses characteristic of newly generated GCs (*14*, *28*), we compared the strength and kinetics of direct inhibition onto 4-WPI and mature GCs. We found that direct perisomatic inhibition was slower in immature than mature GCs, whereas no differences were found for dendritic IPSCs (fig. S5). These findings indicate that the slow disynaptic inhibition kinetics observed after mPP stimulation is due to a slow IPSC rather than to a delayed recruitment of inhibitory neurons.

The observation that few active mPP terminals are sufficient to recruit immature GCs suggests that this neuronal population could respond to most inputs, acting as good integrators of afferent information. On the other hand, mature GCs that display a higher activation threshold may be recruited by specific inputs, acting as better separators (*9*, *20*). We obtained a quantitative assessment of these properties using calcium imaging to detect activation of neuronal ensembles in response to stimulation of two independent mPP inputs (Fig. 4, A to G, and fig. S6). Inputs 1 and 2 were activated separately and recruited distinct neuronal ensembles containing both immature and mature GCs, with some cells shared by both inputs. We define cells activated independently by both inputs as "good integrators." We quantified the input integration capacity as the number of GCs recruited by both inputs, normalized to the total number of cells recruited by inputs 1 and 2. The ability of a neuronal ensemble to integrate inputs increased with stimulus strength as additional mature and immature GCs were recruited by both inputs (Fig. 4H). Immature GCs exhibited higher levels of integration along the entire input range. Thus, input strengths of ~10% resulted in ~20% integration in mature neurons and ~40% integration in 4-WPI GCs. Such enhanced integration capacity was selective for immature neurons because RFP^+ neurons of 8 weeks of age [8 WPI, when functional properties are fully developed (*3*)] displayed similar input integration to RFP^- GCs. Last, the role of inhibition was assessed by means of PTX blockade of GABA-mediated signaling. PTX increased the ability of mature neurons to integrate independent inputs

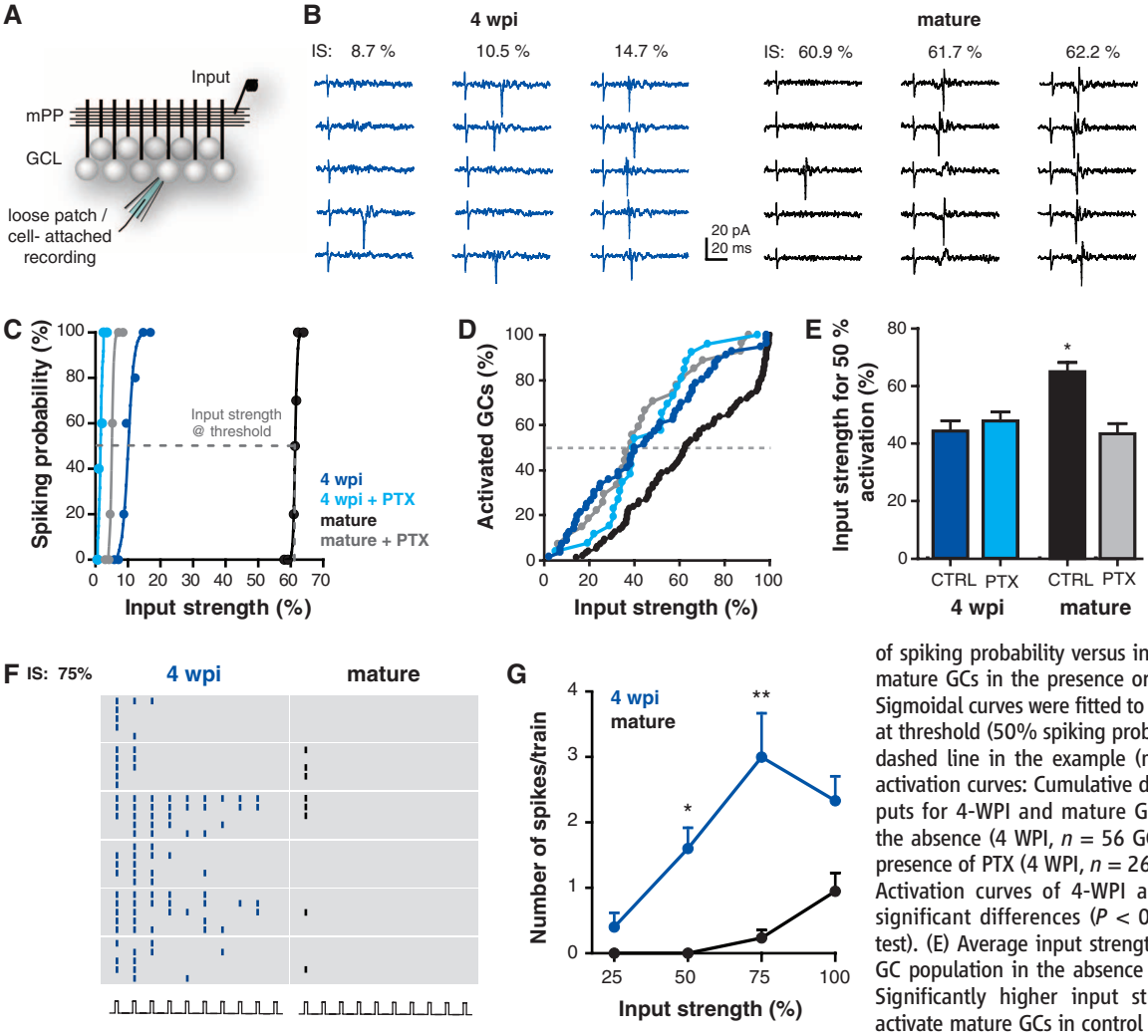

Fig. 2. Differential influence of inhibitory circuits in the activation of immature and mature GCs. (**A** to **E**) Activation of GCs evoked through stimulation of the mPP by single pulses. (A) Schematic diagram depicting the experimental configuration. A stimulating electrode (input) was placed in the mPP, and loose patch recordings were performed to measure spiking probability. (B) Example traces of a 4-WPI and a mature GC recorded at increasing input strengths (IS, normalized to the percent $fEPSP_{slope}$) (fig. S2, A to C). (C) Example curves of spiking probability versus input strength for 4-WPI and mature GCs in the presence or absence of PTX (100 μM). Sigmoidal curves were fitted to calculate the input strength at threshold (50% spiking probability), as indicated by the dashed line in the example (mature GC). (D) Population activation curves: Cumulative distributions of threshold inputs for 4-WPI and mature GC populations recorded in the absence (4 WPI, n = 56 GCs; mature, n = 96 GCs) or presence of PTX (4 WPI, n = 26 GCs; mature, n = 27 GCs). Activation curves of 4-WPI and mature GCs displayed significant differences ($P < 0.006$, Kolmogorov-Smirnov test). (E) Average input strength that recruits 50% of the GC population in the absence (CTRL) or presence of PTX. Significantly higher input strengths were required to activate mature GCs in control conditions than in all other groups (*$P < 0.001$, post-hoc Bonferroni's test after one-way ANOVA). (**F** and **G**) Activation of GCs evoked by stimulation of the mPP at 10-Hz trains. (F) Raster plot depicting spikes recorded from 4-WPI and mature GCs in response to trains (10 pulses, 10 Hz) delivered at 75% input strength (five trials per neuron). (G) Train stimulation elicits a higher number of spikes (mean ± SEM) in 4-WPI GCs than in mature GCs at increasing input strengths. *$P < 0.05$, **$P < 0.001$, after ANOVA and Bonferroni's post-hoc test (n = 7 immature GCs; n = 6 mature GCs).

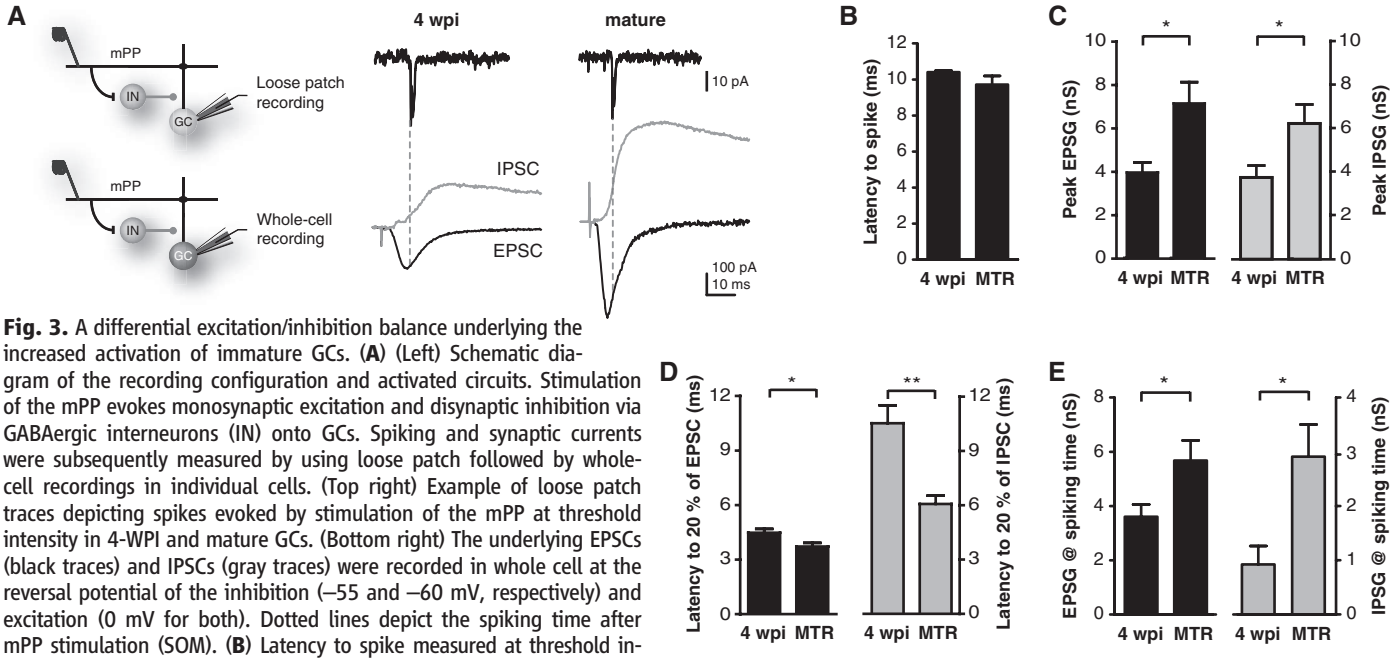

Fig. 3. A differential excitation/inhibition balance underlying the increased activation of immature GCs. (**A**) (Left) Schematic diagram of the recording configuration and activated circuits. Stimulation of the mPP evokes monosynaptic excitation and disynaptic inhibition via GABAergic interneurons (IN) onto GCs. Spiking and synaptic currents were subsequently measured by using loose patch followed by whole-cell recordings in individual cells. (Top right) Example of loose patch traces depicting spikes evoked by stimulation of the mPP at threshold intensity in 4-WPI and mature GCs. (Bottom right) The underlying EPSCs (black traces) and IPSCs (gray traces) were recorded in whole cell at the reversal potential of the inhibition (−55 and −60 mV, respectively) and excitation (0 mV for both). Dotted lines depict the spiking time after mPP stimulation (SOM). (**B**) Latency to spike measured at threshold intensity displayed similar values between 4-WPI and mature GCs. (**C**) Peak EPSG and IPSG in 4-WPI and mature GCs (*$P < 0.02$, t test). (**D**) Latency to onset for EPSCs and IPSCs show a profound delay in IPSC onset for 4-WPI neurons (*$P < 0.05$, **$P < 0.01$, t test). (**E**) EPSG and IPSG amplitudes measured at the precise time of evoked spikes (*$P < 0.05$ for EPSG and $P < 0.03$ for IPSG, t test); $n = 4$ neurons for all experiments.

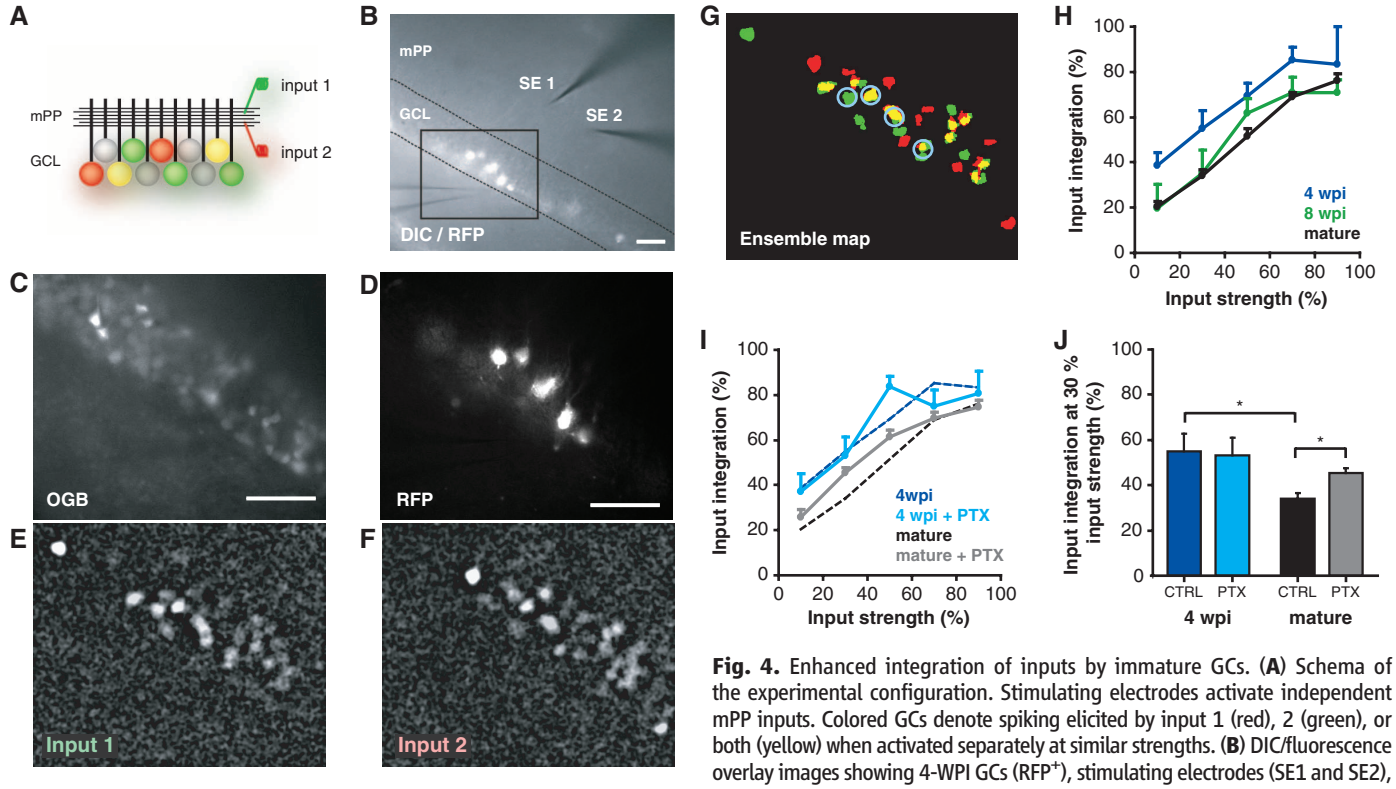

Fig. 4. Enhanced integration of inputs by immature GCs. (**A**) Schema of the experimental configuration. Stimulating electrodes activate independent mPP inputs. Colored GCs denote spiking elicited by input 1 (red), 2 (green), or both (yellow) when activated separately at similar strengths. (**B**) DIC/fluorescence overlay images showing 4-WPI GCs (RFP^+), stimulating electrodes (SE1 and SE2), the extracellular electrode used to assess input independence (fig. S6), and the boxed area used for imaging. (**C** and **D**) Imaged area depicting (C) OGB-1AM loaded cells and (D) RFP^+ GCs. (**E** to **G**) Representative experiment displaying neuronal ensembles activated by (E) input 1 and (F) 2 at similar strengths. Neurons responding to either stimulus (green, red) or both (yellow) are shown in (G) the ensemble map. Blue circles indicate active immature GCs. (**H**) Input integration of recruited ensembles, defined as the proportion of GCs responding to both inputs (activated separately) normalized to the total number of active neurons at each input strength. Input strength was assessed as percent of total activated neurons (fig. S2, D and E, and SOM). Four-WPI GCs ($n = 3$ to 16 slices per bin) displayed higher integration values than those of 8-WPI ($n = 5$ to 13 slices per bin) and mature GCs ($n = 8$ to 34 slices per bin) throughout the curves ($P < 0.01$ for both, two-way ANOVA). Data was binned in 20% intervals. (**I**) Effect of inhibition in input integration. Control curves for 4-WPI and mature GCs [dotted lines, same as in (H)] are plotted for comparison (PTX curves: $n = 3$ to 17 slices per bin, 4-WPI and $n = 11$ to 34 slices per bin, mature GCs). (**J**) Input integration at 30% strength. PTX enhanced integration in mature but not immature GCs (*$P < 0.01$, Bonferroni's test after two-way ANOVA). CTRL, control. Scale bars, 50 μm.

without altering the response of immature neuronal ensembles (Fig. 4, I and J), which is in agreement with our observation that inhibition reduces the activation of mature but not immature GCs (Fig. 2, D and E).

Our data demonstrate that immature GCs exhibit all of the features required to process information and display a low activation threshold due to an enhanced excitation/inhibition balance at the time of spike initiation. At this early developmental stage, they already release glutamate onto CA3 pyramidal cells (fig. S7). As a consequence, neuronal activity in the dentate gyrus is biased toward the immature population of principal neurons that bypass inhibitory control, whereas the activation of mature neurons is limited by inhibition (Figs. 1 and 2 and fig. S8). This is in contrast to other areas of the hippocampus and neocortex, in which inhibition exerts a global (homogeneous) control in the activity of principal cells (*25*, *29*, *30*). Hence, adult neurogenesis emerges as a mechanism that generates a distinct type of network heterogeneity. In addition, the differential control of inhibition revealed here constitutes a simple synaptic mechanism that could underlie the enhanced capacity of immature GCs to undergo activity-dependent synaptic potentiation when GABAergic inhibition is left intact (*12*, *13*, *31*). In the context of the low activation threshold described here, the increased plasticity might provide an efficient means for strengthening and reinforcing weak synaptic inputs that are repeatedly activated during a restricted time window.

The observed network heterogeneity may be crucial for the integration and separation of spatial patterns, properties that have been attributed to the dentate gyrus (*10*). Their low activation threshold and low input specificity make immature GCs appropriate substrates for pattern integration—a feature that has been proposed in computational models of adult neurogenesis (*10*, *18*, *19*, *32*). In this context, immature neurons represent a population of integrators that are broadly tuned during a transient period and may encode most features of the incoming afferent information. When becoming mature, new GCs display a high activation threshold and input specificity and will, therefore, become good pattern separators. Adult neurogenesis would then maintain the renewable cohorts of highly integrative GCs in the dentate gyrus. Last, the functional properties described here support a hypothesis in which activity reaching the dentate gyrus could undergo differential decoding through immature neuronal cohorts that are highly responsive and integrative and, in parallel, through a large population of mature GCs with sparse activity and high input specificity.

References and Notes

1. H. van Praag *et al.*, *Nature* **415**, 1030 (2002).
2. S. Jessberger, G. Kempermann, *Eur. J. Neurosci.* **18**, 2707 (2003).
3. D. A. Laplagne *et al.*, *PLoS Biol.* **4**, e409 (2006).
4. P. M. Lledo, M. Alonso, M. S. Grubb, *Nat. Rev. Neurosci.* **7**, 179 (2006).
5. V. Ramirez-Amaya, D. F. Marrone, F. H. Gage, P. F. Worley, C. A. Barnes, *J. Neurosci.* **26**, 12237 (2006).
6. C. D. Clelland *et al.*, *Science* **325**, 210 (2009).
7. C. O. Lacefield, V. Itskov, T. Reardon, R. Hen, J. A. Gordon, *Hippocampus* **22**, 106 (2012).
8. D. Dupret *et al.*, *PLoS ONE* **3**, e1959 (2008).
9. A. Sahay, D. A. Wilson, R. Hen, *Neuron* **70**, 582 (2011).
10. A. Treves, A. Tashiro, M. E. Witter, E. I. Moser, *Neuroscience* **154**, 1155 (2008).
11. G. L. Ming, H. Song, *Neuron* **70**, 687 (2011).
12. S. Wang, B. W. Scott, J. M. Wojtowicz, *J. Neurobiol.* **42**, 248 (2000).
13. J. S. Snyder, N. Kee, J. M. Wojtowicz, *J. Neurophysiol.* **85**, 2423 (2001).
14. M. S. Espósito *et al.*, *J. Neurosci.* **25**, 10074 (2005).
15. S. Ge, C. H. Yang, K. S. Hsu, G. L. Ming, H. Song, *Neuron* **54**, 559 (2007).
16. C. Schmidt-Hieber, P. Jonas, J. Bischofberger, *Nature* **429**, 184 (2004).
17. L. A. Mongiat, M. S. Espósito, G. Lombardi, A. F. Schinder, *PLoS ONE* **4**, e5320 (2009).
18. S. Becker, J. M. Wojtowicz, *Trends Cogn. Sci.* **11**, 70 (2007).
19. J. B. Aimone, J. Wiles, F. H. Gage, *Neuron* **61**, 187 (2009).
20. J. B. Aimone, W. Deng, F. H. Gage, *Neuron* **70**, 589 (2011).
21. N. Kee, C. M. Teixeira, A. H. Wang, P. W. Frankland, *Nat. Neurosci.* **10**, 355 (2007).
22. A. Tashiro, H. Makino, F. H. Gage, *J. Neurosci.* **27**, 3252 (2007).
23. J. K. Leutgeb, S. Leutgeb, M. B. Moser, E. I. Moser, *Science* **315**, 961 (2007).
24. G. Buzsàki, E. Eidelberg, *Brain Res.* **230**, 346 (1981).
25. F. Pouille, A. Marin-Burgin, H. Adesnik, B. V. Atallah, M. Scanziani, *Nat. Neurosci.* **12**, 1577 (2009).
26. L. A. Ewell, M. V. Jones, *J. Neurosci.* **30**, 12597 (2010).
27. S. Ge *et al.*, *Nature* **439**, 589 (2006).
28. S. J. Markwardt, J. I. Wadiche, L. S. Overstreet-Wadiche, *J. Neurosci.* **29**, 15063 (2009).
29. N. J. Priebe, D. Ferster, *Neuron* **57**, 482 (2008).
30. C. Poo, J. S. Isaacson, *Neuron* **62**, 850 (2009).
31. S. Ge, K. A. Sailor, G. L. Ming, H. Song, *J. Physiol.* **586**, 3759 (2008).
32. J. B. Aimone, J. Wiles, F. H. Gage, *Nat. Neurosci.* **9**, 723 (2006).

Acknowledgments: We thank M. Veggetti for technical assistance, S. Ge for the channelrhodopsin-2 viral construct, and B. Aimone, Y. Li, F. Gage, and M. Scanziani for insightful discussions. A.M.B., L.A.M., and A.F.S. are investigators of the National Research Council (CONICET). M.B.P. was supported by a CONICET fellowship. This work was supported by the Guggenheim Fellowship and by grants from the National Institutes of Health (FIRCA R03TW008607-01), the Howard Hughes Medical Institute (grant 55005963), and the Agencia Nacional de Promoción Científica y Tecnológica PICT2008 to A.F.S. and PICT2010 to A.M.B. and A.F.S.

Supporting Online Material

www.sciencemag.org/cgi/content/full/science.1214956/DC1
Materials and Methods
Figs. S1 to S8
References

7 October 2011; accepted 13 January 2012
Published online 26 January 2012;
10.1126/science.1214956

Unique Processing During a Period of High Excitation/Inhibition Balance in Adult-Born Neurons

Antonia Marín-Burgin, Lucas A. Mongiat, M. Belén Pardi and Alejandro F. Schinder (January 26, 2012)

Science **335** (6073), 1238-1242. [doi: 10.1126/science.1214956] originally published online January 26, 2012

Editor's Summary

Neurogenesis and Pattern Integration

The adult hippocampus continuously produces new neurons that integrate into the dentate gyrus network and contribute to information processing. What features of adult-born neurons are important for information processing in the dentate gyrus? **Marín-Burgin *et al.*** (p. 1238, published online 26 January; see the Perspective by **Kempermann**) labeled newborn neurons and used sophisticated electrophysiological and imaging techniques to show that immature neurons integrated a broader variety of synaptic inputs from different origins compared with mature neurons, which were highly input specific. Thus, immature neurons may represent a population of integrators that are broadly tuned during a transient period and may encode most features of incoming information. After maturation, new granule cells display a high activation threshold and input specificity to become good pattern separators.

Science (print ISSN 0036-8075; online ISSN 1095-9203) is published weekly, except the last week in December, by the American Association for the Advancement of Science, 1200 New York Avenue NW, Washington, DC 20005.